Computational Heat Transfer and Two-phase Flow in Miniature Tubes

D. Lakehal and C. Narayanan

ASCOMP GmbH, Zurich, Switzerland, lakehal@ascomp.ch; chidu@ascomp.ch

ABSTRACT

Detailed computational microfluidics flow simulations have been performed to study the effect of two-phase flow regime on heat transfer in small pipes. We essentially show that only with interface tracking methods such as the Level Set employed here can the coupled heat-fluid flow problems well predicted, with detailed information about the physics of the transfer in tube confines. Overall the heat removal rate in two-phase flow is higher than in single phase. Subtle differences in thermal removal rates are revealed when flow-regime transition is triggered from bubbly to slug configuration.

Keywords: Level sets, heat transfer, CFD, MEMS

1 INTRODUCTION

Miniature pipes can now be exploited to make micro-cooling devices for electronic components (e.g. laptops, computer chips, cellular phones, etc.), radar and aerospace avionics. The physics of two-phase flow in tubes of this scale is multifaceted, featuring significant differences with macroscale transport phenomena. The differences concern pressure and temperature drop, friction coefficient, velocity profile, and heat removal rate. More subtle differences are rooted into the unbalance between surface forces, which dominate with decreasing tube size, and body forces. The high ratio of total surface area to volume, characterising microchannels, is useful in facilitating the removal of a large amount of heat from the tube confines. Also, the use of convective boiling is particularly desirable for increasing heat removal efficiency, as the latent heat of vaporization is appreciably higher than sensible heat changes for a set of temperature operating ranges.

The ability to predict the physics of microfluidics and associated heat transfer in miniature tubes is essential for various emerging technologies, including ink-jet electro-thermal systems, MEMS design, chip cooling and medical diagnostics devices. In practical applications, the flow may involve phenomena acting at different time/length scales. At each level of the scale cascade, the physics of the flow is amenable to numerical prediction by scale-specific strategies. The simulation approach should typically be capable of predicting flow motion and topology; inter-phase transfer mechanisms; capillary forces; and other thermal effects (e.g. Marangoni). Only with such capabilities could the physics of microfluidics be accurately predicted.

In this paper we report on the way this class of flow is tackled by use of the Level Set approach [1], in which we have incorporated phase-change capabilities [2], surface tension and triple-line dynamics models based on the Young's unbalanced forces [3]. The focus here is on the role played by flow regime in controlling heat transfer. We will show that a tiny change in the gas-phase Reynolds number can trigger flow regime transition from bubbly-slug to a bubbly, which in turn leads to an increase in local heat transfer. The 2D axisymmetric simulations were performed in a 1mm diameter tube heated at the surface, in which air bubbles were injected into water stream. The computational strategy combines the unsteady Navier-Stokes equations for the flow and Level Sets for interface dynamics. The experimental data used as reference are extracted from [4].

2 SIMULATION FRAMEWORK

2.1 TransAT© Microfluidics Code

The CFD code TransAT© [2] is a macro/microfluidics, multi-physics, finite-volume code based on solving multi-fluid Navier-Stokes equations. The one-fluid formulation context on which TransAT© is built is such that the flow is supposed to involve in one fluid having variable material properties, which vary according to the color function as it is advected by the mean flow, identifying gas flow regions from the liquid phase. Specifically, both the Level-Set and the Volume of Fluid Interface Tracking Methods (ITM) [5] can be employed in the code to track evolving interfaces.

2.2 Interface Tracking Context

When the exact shape of the interfaces separating two fluids is not known, or not relevant, one may resort to the averaged Two-Fluid approach, where separate conservation equations are required for each phase with appropriate interfacial exchange forces. ITM's may be invoked when the identification of interfaces needs to be precise, as in the breakup of large bubbles, droplets or liquid jets. The key to the methods is the use of a single-fluid set of conservation equations with variable material properties and surface forces. The concept is attractive, since it offers the prospect of a more subtle strategy than that offered by the two-fluid formalism, while minimizing modeling assumptions.

2.3 Transport Equations

The incompressible thermo-fluidics equations expressed within the single-fluid formalism take the following form

$$\nabla . u = 0 \qquad (1)$$

$$\partial_t(\rho u) + \nabla.\left(\rho\, u\, u - \sigma\right) = F_s + F_g + F_w \quad (2)$$

$$\partial_t(\rho e) + \nabla.\left(\rho\, e\, u - q''\right) = \sigma : \nabla u + S_h \quad (3)$$

where the RHS terms in the momentum equation represent the body forces, the surface tension expressed by Eq. (5) below, and its triple-line wall contribution [3], respectively. In Eqs (2-3) where phase change is not accounted for, σ is the Newtonian stress tensor, e is the internal energy, q'' is the heat flux, and S_h is the volumetric heat source.

In the LS method employed here the interface between immiscible fluids is represented by a continuous function ϕ, representing the distance to the interface that is set to zero on the interface, is positive on one side and negative on the other. This way, both fluids are identified, and the location of the physical interface is associated with the zero level. The LS evolution equation is given by

$$\partial_t \phi + u\, \nabla \phi = 0 \quad (4)$$

Material properties such as the density, the viscosity, the conductivity are updated locally based on ϕ, and smoothed across the interface using a modified Heaviside function. Further, the fact that ϕ is a continuous function across the interface helps determine the normal vector **n** to the interface, and thereby the surface curvature κ required for the determination of the surface tension,

$$F_s = \gamma\, \kappa\, n\, \delta_s + \left(\nabla_s \gamma\right) \delta_s \quad (5)$$

where γ is the surface tension coefficient of the fluid. The second term in the RHS expresses the Marangoni effects, translating the interfacial change in γ with temperature. This feature does not apply in this work.

In practice the level set function ceases to be the signed distance from the interface after a single advection step of Eq. (4). To restore its correct distribution near the interface, a *re-distancing* problem has to be solved, in which the equation below has to be integrated to steady state:

$$\partial_\tau d - \mathrm{sgn}(d_0)(1 - |\nabla d|) = 0; \quad d_0(x,t) = \phi(x,t) \quad (6)$$

Equation (6) is solved after each advection step of Eq. (4), using the non-oscillatory 3rd-order WENO scheme. The Navier-Stokes transport equations and the level set advection function are solved using the 3rd order Runge-Kutta explicit scheme for time integration of all variables. The convective fluxes are discretised using the 3rd order Quick scheme bounded using a TVD limiter. The diffusive fluxes are differenced using a 2nd order central scheme.

3 THERMAL FLOW IN SMALL TUBES

3.1 The Experiment and CFD Set-ups

The data used for reference in this work are taken from Chen *et al.*'s experiment [4], which was conducted without heat transfer. In that campaign, air-water flow was pumped at various flow rates in a closed loop into a 1mm diameter pipe. Three flow regimes were investigated: bubbly, slug, and churn. The measurements provide the exact void fractions for specific inlet mass flow rates, which help set the flow boundary conditions in computations.

The simulations were conducted under axisymmetric conditions in 1 x 10-15 mm tubes for single and two-phase flow. The inlet flow conditions were extracted from experiments; the pipe was heated from below at a constant temperature ($T_w = 340^0$K). No-slip conditions were applied at the wall. Buoyancy forces were neglected. The triple-line wall model was not activated. The final grid resolution for single phase consisted of a 40x200 nodes, which permitted to resolve well the velocity and thermal boundary layers. All two-phase flow simulations required more refined grids of 60x460 nodes. The liquid Reynolds number based on pipe diameter was $Re_L = 1111$, and the gas inflow velocity 0.66m/s. Specific void fractions α are listed in Table 1.

3.2 Flow Transition Results

Figure (1) depicts the thermal flow behavior in both the pure water and bubbly/slug flow regimes. The colored isocontours refer to the thermal field; the black line indicates the interface location. The upper panel of the figure shows the steady state conditions reached, and the thermal boundary layer development far downstream. The lower panel shows the onset of slug formation from the slug-train dislocation. The ability of the code to predict such fragmentation highlights its performance, robustness and stability in treating high-density ratio microfluidics flows, and more precisely the way surface forces are handled. This performance is remarkable insofar as it is achieved for coarse grids used for typical design purposes. The figure clearly reveals the strong interaction between the slug and the wall, dragging a substantial heat rate down to the core-flow region

The inverse flow transition mechanism is illustrated in Fig. (2), where an initial plug/slug of air is gradually penetrating the water tube to form of a long slug train. In contrast to the previous scenario, here the main credit is due to the wall dynamic contact angle treatment in momentum equations, which allows capturing such flow transition.

3.3 Heat Transfer Results

Figure (3) presents post-fragmentation sequences of the flow taken in the fully developed region at X/D = 7 and 12. The first figure shows the first slug forming after the dislocation of the main train, that occurs at X/D = 5. The heat diffuses first from the wall down starting from the frontal surface of the slug. As the slug grows in scale and gets closer to the wall, the heat is transferred from the high-curvature rear circumference.

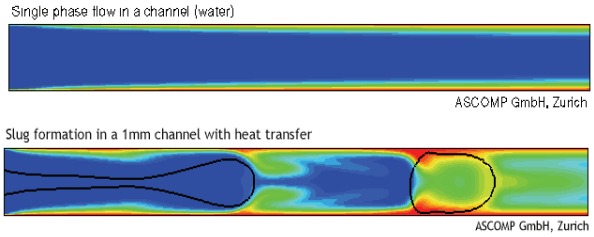

Figure 1: Heat transfer prediction in water and slug flow. Flow regime transition from train to slug.

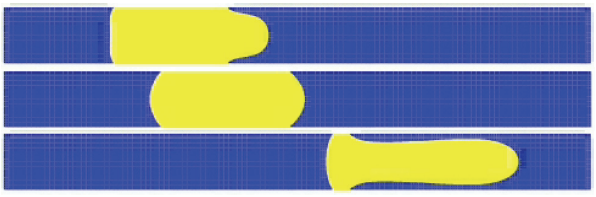

Figure 2: Inverse flow transition from slug to train.

It is interesting to note that the maximum heat removal rate takes place at this location. The heat removal main mechanism is essentially a convective transport taking place at the rear of the slug, where high curvature surfaces approach the wall. A jet-like flow forms there and penetrates the inclusion, transporting heat into the core. The thermal field gradually penetrates the entire slug to form an unstable thermal stratification. The interfacial area of the slug helps exchange a larger portion of heat between the fluids, as compared to the bubbly flow discussed next.

Figures (4) presents similar bubbly flow scenarios taken at X/D = 3 and 7, after the initial train is broken at X/D = 2 into bubble trains then slugs. The figure shows that at their birth, the inclusions are first slugs, then take the shape of bubbles only far downstream at X/D = 7. Although the thermal boundary layer does not seem to be affected by the inclusion, or slightly at the early stage of the train, the results of the heat transfer rates discussed in the context of Table 1 indicate the contrary. Compared to the slug-flow regime results shown before, the heat penetration in the bubble core flow is less pronounced, which is well illustrated in Fig. 5, comparing temperature profiles. The difference between heat penetrations into the bulk represents about 20% of the total subcooling rate.

The visual difference between slug and bubby flow regimes, when inspecting Figs. (3 and 4), is the thickness of the thermal boundary layer. It seems indeed that the bubble exercises a higher confinement or blockage effect than the slug flow, translated into a thinner thermal boundary layer (c.f. Fig. 5), which should eventually promote wall heat transfer. Clearly, the bubbly flow induces a larger heat flux than the slug; both being larger than the pure water flow.

More insight into the boundary layer development is gained by looking at Fig. 6, comparing the velocity profiles. The slopes of these profiles deviate from the thermal ones because of the water Prandtl number is larger than unity.

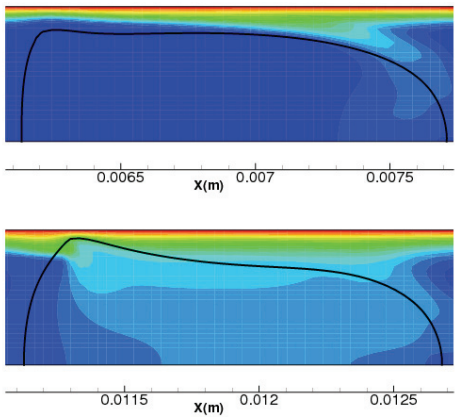

Figure 3: Slug formation and heat transfer at 2 locations.

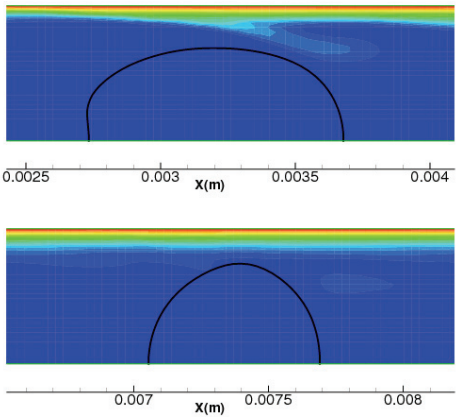

Figure 4: Bubble formation and heat transfer at 2 locations.

The structure of the flow inside the inclusions are also different, in that a reverse flow forms in the slug, trapping heat longer within the cell. This explains why, in average, scalar penetration in the bulk is larger than in bubbly flow.

Figure (7) compares the Nusselt number distributions along the axis for single and two-phase flow regimes. The bulk temperature is conveniently taken to be the average centerline temperature along the axis. The local Nusselt number $\boldsymbol{Nu_x}$ and the wall heat flux $\boldsymbol{q''_w}$ are defined by

$$Nu_x = \frac{q''_w|_x}{\left(T_w|_x - T_\infty\right)}\frac{D}{k}; \quad q''_w|_x = k\left.\frac{\partial T}{\partial n}\right|_w \qquad (7)$$

The water flow results corroborate with the Hagen-Poiseuille flow solution, according to which, Nu asymptotes towards 3.66. The slug flow data show large fluctuations around the mean value 7.5. The maximum value 12.7 is reached where the train breaks up (X/D = 5). The successive sub-harmonics translate the passage of individual slugs, or more precisely their wall-adjacent, rear circumferences, as discussed previously.

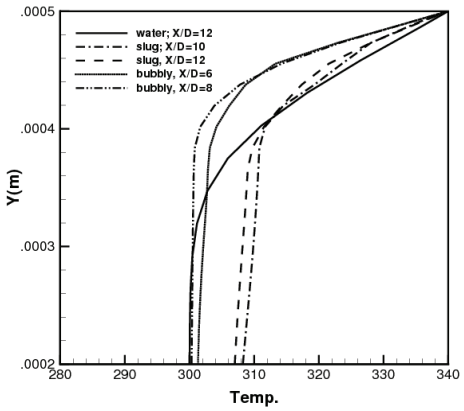

Figure 5: Predicted heat profiles at various locations.

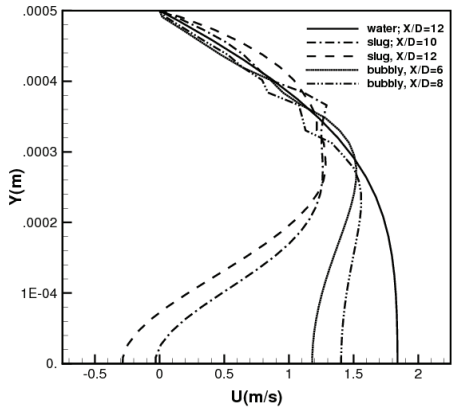

Figure 6: Predicted velocity profiles at various locations.

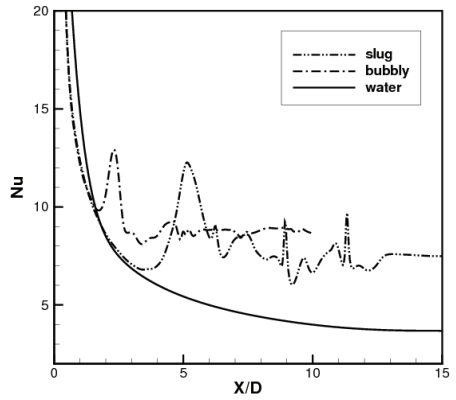

Figure 7: Nusselt number distribution along the axis.

Lower fluctuations are observed in the bubbly flow signal, however, though a marked peak (Nu = 13) is visible, corresponding to the initial breaking location (X/D = 2). Overall the average Nusselt number is twice as high in the two-phase flow regimes. The bubbly flow removes more heat due to its large blockage effects.

Table 1 compiles typical heat transfer rate data for all flow simulations. The wall heat flux (***q"****) is normalized by that of pure water. The quantities reported were taken in the fully developed flow region, at the center of three individual slugs and bubbles (as in Figs. 3 and 4). The mean Nusselt number is statistically defined using local values in the fully developed region. As discussed above, the water flow simulation provides a Nusselt number perfectly in line with the analytical data. The local Nu numbers taken at the center of individual inclusions are larger than in the water, but smaller than the means. Also, the slug flow results are higher than for the single-phase value [6], i.e. Nu = 5.78.

CASE STUDY	α	Nu_x	Nu_{mean}	$q"^*$
Water	0.0	3.67	3.67	1
Slug	0.3634	6.92	7.5	1.42
Bubbly	0.1965	7.94	8.6	1.92

Table 1: Flow conditions (void α) and heat transfer data.

4 CONCLUSIONS

Detailed computational microfluidics flow simulations have been performed to study the effect of varying flow regime on the heat transfer in small tubes. Interface tracking methods were employed for the purpose, providing local detailed information about heat transfer. Overall the heat removal rate in two-phase flow is higher than in single phase. Subtle differences were revealed between slug flow, which dissipates more heat in the bulk, and bubbly flow, which has a higher wall heat flux due a pronounced blockage effect. From an engineering standpoint, such direct computational microfluidics are necessary, and will pave the way to transcend the era of empiricism to knowledge-based design for new technologies and systems.

REFERENCES

[1] M. Sussman, P. Smereka and S. Osher, J. Comp. Physics, 30, 969, 1996.
[2] TransAT© User Manual: www.ascomp.ch
[3] H.M. Friess and D. Lakehal, Comp. Heat Transfer 4 (CHT04), Kirkenes, Norway, 19-24 April, 2004.
[4] W.L. Chen, M.C. Twu and C. Pan, Int. J. Multiphase Flow. 28, 1235, 2002.
[5] D. Lakehal, M. Meier and M. Fulgosi, Int. J. Heat & Fluid Flow, 23, 242, 2002.
[6] E.M. Sparrow and S.V. Patankar, J. Heat Transfer, 99, 483, 1997.